Supreet Singh Bahga[1]
Prateek Gupta[2]

[1]Department of Mechanical Engineering, Indian Institute of Technology Delhi, New Delhi, India
[2]Department of Applied Mechanics, Indian Institute of Technology Delhi, New Delhi, India

Received September 7, 2021
Revised December 4, 2021
Accepted December 6, 2021

Research Article

Electrophoresis simulations using Chebyshev pseudo-spectral method on a moving mesh

We present the implementation and demonstration of the Chebyshev pseudo-spectral method coupled with an adaptive mesh method for performing fast and highly accurate electrophoresis simulations. The Chebyshev pseudo-spectral method offers higher numerical accuracy than all other finite difference methods and is applicable for simulating all electrophoresis techniques in channels with open or closed boundaries. To improve the computational efficiency, we use a novel moving mesh scheme that clusters the grid points in the regions with poor numerical resolution. We demonstrate the application of the Chebyshev pseudo-spectral method on a moving mesh for simulating nonlinear electrophoretic processes through examples of isotachophoresis (ITP), isoelectric focusing (IEF), and electromigration-dispersion in capillary zone electrophoresis (CZE) at current densities as high as 1000 A/m^2. We also show the efficacy of our moving mesh method over existing methods that cluster the grid points in the regions with large concentration gradients. We have integrated the adaptive Chebyshev pseudo-spectral method in the open-source SPYCE simulator and verified its implementation with other electrophoresis simulators.

Keywords:
Adaptive grid / Electrophoresis simulations / Pseudo-spectral method
DOI 10.1002/elps.202100279

Additional supporting information may be found online in the Supporting Information section at the end of the article.

1 Introduction

Numerical simulations have found increasing utility in design, optimization, and understanding the dynamics of electrophoresis techniques. With the advances in mathematical modeling of electrophoretic phenomena, numerical methods, and computing power over the past four decades [1, 2], realistic simulations of electrophoresis techniques such as capillary zone electrophoresis (CZE) [3], isotachophoresis (ITP) [4], transient-ITP (t-ITP) [5], isoelectric focusing (IEF) [6], and field amplified sample stacking (FASS) [7] can now be performed on personal computers. Moreover, the availability of open-source electrophoresis simulators such as SIMUL [8], SPRESSO [9], and SPYCE [10] and commercial multiphysics simulation packages such as COMSOL [11] have popularized the use of simulations for research and teaching activities.

Electrophoresis simulations are based on solving coupled, mass conservation equations for ionic species in an electrolyte. These conservation equations include mass-fluxes due to electromigration, bulk advection, and molecular diffusion, and also account for acid–base equilibria. The species transport equations for electrophoretic transport of weak electrolyte species were originally formulated by Bier et al. [12] and Saville and Palusinski [13]. All electrophoresis simulators are based on the same basic mathematical model, usually simplified to a one-dimensional (1D) setting. However, over time various improvements to this mathematical model have been made and incorporated in different simulators, such as ionic-strength dependence on electrophoretic mobility [14], modeling of protein mobility [15], Taylor–Aris dispersion [9, 16], and axially varying channel cross-section [16]. The governing equations for electrophoretic transport can be solved numerically using various approaches such as finite-difference, finite-volume, and finite-element methods. These simulation approaches and progress in modeling of electrophoresis techniques have been reviewed in detail by Thormann et al. [1, 2].

Correspondence: Supreet Singh Bahga, Department of Mechanical Engineering, Indian Institute of Technology Delhi, New Delhi, India.
E-mail: bahga@mech.iitd.ac.in

Color online: See article online to view **Figs. 1–3** in color.

A majority of electrophoresis simulations are based on spatial-discretization schemes having second-order accuracy. In particular, electrophoresis simulators such as SIMUL [8] and GENTRANS [17] are based on the second-order central differencing scheme. The SPRESSO simulator [9, 16] offers a choice between the sixth-order compact finite difference scheme and other first- and second-order accurate spatial-discretization schemes. These finite-difference and finite-volume schemes are based on locally approximating the spatially varying physical quantities using low-order polynomials. Recently, we demonstrated the use of the Fourier pseudo-spectral method for performing high-resolution electrophoresis simulations, and based on it, we developed a new simulator named SYPCE [10]. Unlike the finite-difference and finite-volume methods, the pseudo-spectral methods offer exponential convergence as they are based on global representations of a function using the Fourier series or high-order polynomials [18, 19]. As shown by Fornberg [20], the pseudo-spectral methods can be considered as the limit of finite-difference methods with infinite order of accuracy. Consequently, pseudo-spectral methods yield accurate numerical solutions on coarser computational grids and correspondingly require lower computational time than other spatial-discretization schemes.

Previously, we reported the use of the Fourier pseudo-spectral method for performing fast and accurate electrophoresis simulations and demonstrated its advantages over finite-difference methods in terms of speed and accuracy [10]. Because the Fourier pseudo-spectral method is based on Fourier series representation of spatially varying physical quantities, it is applicable for performing simulations only on a periodic domain. Despite the requirement of periodicity, we showed that the Fourier pseudo-spectral method could be used to simulate a variety of electrophoresis processes, such as CZE, FASS, oscillating electrolytes [21, 22], and t-ITP, as the conditions at the left and the right channel (or computational domain) boundaries in these electrophoresis techniques are identical. However, several electrophoresis techniques such as ITP and IEF cannot be simulated on a periodic domain, as these techniques involve different ionic species on the channel boundaries.

In the current work, we show that nonperiodic electrophoresis problems can be simulated using the pseudo-spectral method based on Chebyshev polynomials to represent the spatially varying quantities, instead of the Fourier series. To this end, we present the implementation of the Chebyshev pseudo-spectral method for simulating electrophoretic processes and demonstrate its applicability for simulating ITP, IEF, and other electrophoresis techniques. The Chebyshev pseudo-spectral method overcomes the limitations of the Fourier pseudo-spectral method and is applicable for simulating all practical electrophoresis techniques, irrespective of whether the channel boundaries are open or closed. To improve the stability and the computational speed of the numerical method, we also incorporate a moving mesh method in our simulations to dynamically cluster the grid points in the regions prone to numerical errors. The Chebyshev pseudo-spectral method coupled with the moving mesh method yields robust and accurate numerical simulations of electrophoresis techniques with sharp concentration gradients, with fewer grid points and correspondingly lower computational time. Based on this numerical scheme, we have thoroughly updated the open-source SPYCE (Pseudo-spectral Python Code for Electrophoresis) simulator. Consequently, the updated SPYCE simulator is no longer limited to simulations on a periodic domain and can simulate all 1D electrophoresis techniques. SPYCE is available for free download at http://web.iitd.ac.in/~bahga/SPYCE.html along with sample input files for simulating various electrophoresis techniques.

2 Materials and methods

2.1 Mathematical model

We consider electrophoretic transport of ionic species in an electrolyte filled in a uniform cross-section capillary, in the absence of bulk fluid flow due to pressure gradients and electroosmotic slip. We can model the species transport in such electrophoretic systems with a set of coupled 1D mass-conservation equations accounting for electromigration and diffusive fluxes,

$$\frac{\partial c_i}{\partial t} + \frac{\partial}{\partial x}(\mu_i c_i E) = \frac{\partial^2}{\partial x^2}(D_i c_i), \quad i = 1, 2, \ldots, M, \tag{1}$$

Here, c_i denotes the total (analytical) concentration of species family i, E the local electric field, μ_i the effective mobility, D_i the effective diffusivity, and M the total number of species families in the electrolyte. The derivation of these governing equations has been discussed in detail by Saville and Palusinski [13] and Bercovici et al. [9], and we briefly summarize the procedure here. The derivation of these equations involves formulating individual mass conservation equations for different ionization states of each species family, incorporating electromigration and diffusion fluxes and source terms due to acid–base dissociation reactions. After that, the transport equations for all ionization states of a particular species family are summed up to arrive at Equation (1) in terms of the total concentration of the species family. Because the mass of every species family is conserved, the source terms due to dissociation–recombination reactions do not appear in Equation (1). Moreover, because acid–base dissociation reactions occur at a significantly shorter timescale than the timescale for electromigration and diffusion, the fractions of a species family in various ionization states can be calculated assuming local chemical equilibrium. The effective mobility μ_i and effective diffusivity D_i in Equation (1) are the weighted averages of mobilities and diffusivities of various ionization states with ionization fractions as the weights. Therefore, knowing the total concentrations of all the species families, acid–base equilibrium equations are solved along with local electroneutrality condition to determine the pH and the

ionization fractions, using which effective mobilities and diffusivities are calculated.

The species transport equations, Equation (1), are coupled through the local electric field E, which depends on the local electrical conductivity σ and thus on concentrations of all species. For a constant current density j, the local electric field is given by

$$E = \frac{1}{\sigma}\left(j + \frac{\partial S}{\partial x}\right), \tag{2}$$

where $\partial S/\partial x$ is the diffusive current density [9]. The conductivity and diffusive current density depend on the species concentrations and local pH, and their expressions are provided in Bercovici et al. [9]. The overall mathematical model for electrophoresis consists of M coupled partial differential equations for species transport and algebraic equations for local acid-base equilibrium and electroneutrality.

2.2 Chebyshev pseudo-spectral method

We solve the governing equations, Equations (1) and (2), using the Chebyshev pseudo-spectral method [18, 19]. In this numerical method, a physical quantity f is approximated on a computational domain $-1 \le \xi \le 1$ by a finite series of Chebyshev polynomials as

$$f(\xi, t) = \sum_{n=0}^{N} a_n(t) T_n(\xi), \tag{3}$$

where $T_n(\xi)$ denotes the n-th Chebyshev polynomial. The first few Chebyshev polynomials are

$$T_0 = 1, \quad T_1 = \xi, \quad T_2 = 2\xi^2 - 1, \quad T_3 = 4\xi^3 - 3\xi, \ldots. \tag{4}$$

In general, the Chebyshev polynomials can be generated using the following recursive relation:

$$T_{n+1}(\xi) + T_{n-1}(\xi) = 2\xi T_n(\xi), \quad n \ge 1. \tag{5}$$

In addition, a one-to-one mapping between the computational coordinate ξ and the physical coordinate x varying over the length of the capillary is defined. This mapping can even be time-varying, $x = x(\xi, t)$ while using a dynamically adapting mesh, as discussed later in Section 2.3.

The Chebyshev polynomials have an important property that they can be expressed as simple cosines through the transformation $\xi = \cos\theta$, which yields $T_n(\cos\theta) = \cos n\theta$. Therefore, the linear combination of Chebyshev polynomials in Equation (3) can be expressed as a trigonometric series, using this representation of a series of Chebyshev polynomials, the derivative df/dx in the physical domain can be calculated as,

$$f(\xi(\theta), t) = \sum_{n=0}^{N} a_n(t) \cos n\theta,$$

$$\text{where } \theta = \cos^{-1}\xi, \quad 0 \le \theta \le \pi. \tag{6}$$

$$\frac{df}{dx} = \frac{1}{dx/d\xi}\frac{df}{d\theta}\frac{d\theta}{d\xi} = \frac{1}{dx/d\xi\sqrt{1-\xi^2}}\frac{df}{d\theta}. \tag{7}$$

Here, $dx/d\xi$ is known from the mapping between the physical and computational coordinates. The derivative $df/d\theta$ can be efficiently computed using the Fast Fourier Transform (FFT) algorithm from the discrete values of f at varying θ, similar to that in the Fourier pseudo-spectral method [18]. To use FFT to compute the derivative $df/d\theta$ numerically, the computational domain $-1 \le \xi \le 1$ is discretized using the Chebyshev points,

$$\xi_j = \cos(j\pi/N), \quad j = 0, 1, \ldots, N, \tag{8}$$

which correspond to non-uniformly spaced grid points along ξ coordinate, but equispaced grid points $\theta_j = j\pi/N$ along the θ-coordinate. After computing $df/d\theta$, the derivative in physical space df/dx can be calculated using Equation (7) with special formulae for the endpoints, $\xi = \pm 1$. The complete algorithm for Chebyshev spectral differentiation has been described by Trefethen [18], and we adopted the same algorithm in the current work.

2.3 Moving mesh method

The Chebyshev grid points given by Equation (8) are clustered near the boundaries, and the grid density is the lowest in the middle of the computational domain. Such a grid is not only unsuitable for resolving the concentration gradients within the computational domain but also offers severe time-step restrictions for time-integration of the discretized transport equations [19, 23]. One approach to overcome these issues is to define a fixed mapping $x = x(\xi)$ to distribute the grid points more evenly over the physical domain. A common choice for such a mapping is the arcsine map introduced by Kosloff and Tal-Ezer [23],

$$x = \frac{L}{2}\left(1 + \frac{\arcsin(\beta\xi)}{\arcsin\beta}\right), \tag{9}$$

where $0 \le \beta < 1$, $0 \le x \le L$ for $-1 \le \xi \le 1$, and L is the length of the physical domain, which in the current case is the channel or column. The grid spacing in the physical domain becomes increasingly uniform as $\beta \to 1$, for example, by choosing $\beta = 0.999$.

The arcsine map given by Equation (9) is suitable for simulating electrophoretic processes with relatively small concentration gradients or for processes, such as IEF, where a large number of concentration gradients are distributed throughout the physical domain. However, certain electrophoretic processes such as ITP and electromigration-dispersion in CZE are characterized by sharp concentration gradients localized at a few locations, while the species concentrations vary gradually elsewhere. Such electrophoresis problems can be simulated more efficiently by dynamically adapting the grid by drawing the grid points from regions with low concentration gradients and clustering them in the regions with high concentration gradients [9]. To this end, we define a time-dependent mapping $x = x(\xi, t)$ between the physical coordinate x and the computational coordinate ξ. In

the moving grid framework, the time-derivative term in Equation (1) has an additional term due to the grid movement,

$$\frac{\partial}{\partial t}c_i(x,t) = \frac{\partial}{\partial t}c_i(\xi,t) - \frac{x_t}{x_\xi}\frac{\partial}{\partial \xi}c_i(\xi,t), \tag{10}$$

where $x_t = \partial x/\partial t$ and $x_\xi = \partial x/\partial \xi$. Therefore, the governing equations, Equations (1) and (2), get modified to

$$\frac{\partial c_i}{\partial t} - \frac{x_t}{x_\xi}\frac{\partial c_i}{\partial \xi} + \frac{1}{x_\xi}\frac{\partial}{\partial \xi}(\mu_i c_i E) = \frac{1}{x_\xi}\frac{\partial}{\partial \xi}\left(\frac{1}{x_\xi}\frac{\partial}{\partial \xi}(D_i c_i)\right),$$
$$i = 1, 2, \ldots, M, \tag{11}$$

and

$$E = \frac{1}{\sigma}\left(j + \frac{1}{x_\xi}\frac{\partial S}{\partial \xi}\right). \tag{12}$$

To obtain the time-dependent mapping $x = x(\xi, t)$, we adopt the moving mesh method for pseudo-spectral methods, described by Subich [24]. In this method, the time-varying mapping $x = x(\xi, t)$ is determined by solving the following partial differential equation:

$$\frac{\partial^2}{\partial \xi^2}\left(\frac{\partial}{\partial t}x(\xi,t)\right) = -\frac{1}{\tau}\frac{\partial}{\partial \xi}\left(\sqrt{1-\xi^2}M(\{c_i(x,t)\})\frac{\partial}{\partial \xi}x(\xi,t)\right), \tag{13}$$

subject to the boundary conditions $x(-1, t) = 0$ and $x(1, t) = L$. In this equation, τ is a positive constant that governs the speed of grid adaptation. A lower value of τ leads to faster grid adaptation. In Equation (13), $M(\{c_i(x, t)\})$ is the so-called monitor function that depends on the species concentrations and governs the clustering of the grid points in the physical domain. The grid points cluster in the regions where the monitor function M takes on higher values, and the grid density reduces in the regions having lower values of M.

Typically, in moving mesh methods, the monitor function is chosen as a function of the spatial gradient of the physical quantity (concentration gradient in the current case). Consequently, the grid points move from the regions with low gradients and cluster at large gradients [25, 26]. However, in the current work, we follow the approach of Subich [24] to construct a monitor function that clusters the grid points in the regions with poorly resolved numerical solution. To construct such a monitor function, we first use a high-pass filter defined by Subich [24] to obtain the high spatial-frequency component $c_{i,high}(x(\xi), t)$ of species concentrations $c_i(x(\xi), t)$. At every grid point, the maximum value of $c_{i,high}(x(\xi), t)$ among all species is taken, and the monitor function is then defined as

$$M(\{c_i(x,t)\}) = \delta + \max_i c_{i,high}(x(\xi),t). \tag{14}$$

The parameter δ governs the relative importance given to regions with high spatial-frequency content in the mesh adaptation process. Lower values of δ lead to higher grid density in the regions with poorly resolved solution, that is, where the solution has high-frequency content. On the other hand, high values of δ yield almost equispaced grid points in the physical domain. In practice, the monitor function defined by Equation (14) is normalized by its maximum value, although its absolute value does not affect the grid density. The resulting normalized monitor function is highly oscillatory, and therefore before using it in Equation (13), we smooth the monitor function using a weighted moving average filter with a triangular weighting function. This smoothing process can be implemented efficiently through FFT-based convolution of the monitor function with a triangular function. In the current work, we used a triangular weighting function spanning 21 grid points for smoothing the monitor function.

The monitor function described above is more robust in adapting the grid than the monitor functions based on concentration gradients [24]. In particular, this monitor function avoids unnecessary clustering of grid points in the regions with well-resolved concentration gradients. Knowing the monitor function $M(\{c_i(x, t)\})$, we solve the governing equation, Equation (13), for the mapping $x = x(\xi, t)$ using the arcsine map given by Equation (9) as the initial condition. We use the Chebyshev spectral differentiation to compute the spatial derivatives in Equation (13), as described by Subich [24].

2.4 Boundary conditions, time-integration, filtering

The governing equations for species concentration, Equations (11) and (12), and the moving mesh Equation (13) are semi-discretized by computing the spatial derivatives using Chebyshev spectral differentiation. For electrophoresis problems with fixed concentrations at the channel boundaries, the time-derivative of species concentrations at the domain boundaries are set to zero. On the other hand, to simulate electrophoretic transport in a domain with impenetrable boundaries, such as in IEF in a closed-column, the mass-flux at the boundaries is set to zero. The ODEs resulting from semi-discretization of species concentrations and the mapping $x(\xi)$ at all the grid points are solved using the fourth-order Runge–Kutta–Fehlberg (RKF45) adaptive time-stepping scheme. The species concentrations from the previous time-step are used once to calculate the pH and effective mobilities and diffusivities at each time-step. Similarly, the grid adaptation speed $\partial x/\partial t$ is also calculated only once for the time-step. The same values of pH, effective mobilities and diffusivities, and grid adaptation speed are used throughout the time-step.

The nonlinear terms in Equation (11) lead to aliasing errors due to the multiplication of the truncated series representations of the concentrations [19]. To avoid aliasing errors, we use the Fourier smoothing method of Hou and Li [27], wherein the discrete Fourier transform coefficients of species concentrations are multiplied with a weighting function to attenuate the high-wavenumber components. Similarly, the mapping between the physical and computational coordinates $x(\xi, t)$ computed using the moving mesh method may not be strictly monotonic in certain regions and hence requires smoothing. Therefore, at the end of every time-step of time-integration, the resulting map $x = x(\xi)$ is smoothed, while preserving the boundary conditions $x(-1) = 0$ and $x(1) = L$. In the current work, we perform

boundary-preserving smoothing of $x(\xi)$ by solving

$$\bar{x} - \varepsilon \frac{d^2\bar{x}}{d\xi^2} = x(\xi), \tag{15}$$

for $\bar{x}$ subject to the boundary conditions $\bar{x}(-1) = 0$ and $\bar{x}(1) = L$. In this equation, $\bar{x}$ is the smoothed mapping and ε is the smoothing parameter. Note that, $\bar{x} \to x$ as $\varepsilon \to 0$. We also solve this boundary value problem using the Chebyshev spectral method [18] using $\varepsilon = 10^{-7}$.

We implemented the numerical algorithm discussed above in the SPYCE simulator, developed using the Python 3.0 programming language with NumPy and SciPy libraries. We verified the numerical implementation by comparing the simulation results for various electrophoresis techniques with SPRESSO, SIMUL, and COMSOL simulators. All simulations were performed on Intel i7 3.6 GHz, 16 GB RAM personal computer with Linux (Ubuntu) operating system.

3 Results and discussion

The adaptive Chebyshev pseudo-spectral method discussed in Section 2 is suitable for simulating all 1D electrophoresis techniques. The advantages of the Chebyshev pseudo-spectral method over lower-order methods are well documented in the literature [18, 19]. The focus of this section is to demonstrate the application of this method for performing electrophoresis simulations on a nonperiodic domain, which otherwise cannot be performed using the Fourier pseudo-spectral method [10]. Here, we consider two test cases of ITP and IEF, which correspond to different boundary conditions for species concentrations at the channel ends. ITP involves fixed species concentrations at the channel ends, whereas in IEF the channel boundaries are impenetrable when performed in a closed column. ITP and IEF serve as challenging simulation test cases as they both involve sharp concentration gradients. Moreover, the ITP simulation case helps in demonstrating the use of the moving mesh method in simulating sharp propagating concentration gradients with relatively less number of grid points. In contrast to ITP, the IEF simulation is a test case where the adaptive grid is of little benefit as the concentration gradients are distributed throughout the domain. We also verify the numerical implementation of the Chebyshev pseudo-spectral method in SYPCE by comparing the ITP simulation with that using SPRESSO and IEF simulation with the predictions of COMSOL Multiphysics package. In addition to the simulations of ITP and IEF presented here, in the Supporting Information, we provide a detailed comparison of accuracy and computational time of SPYCE with SIMUL, SPRESSO, and COMSOL simulators based on simulations of CZE. We show that the Chebyshev pseudo-spectral method implemented in SPYCE has significantly higher numerical accuracy than the numerical methods incorporated in other electrophoresis simulators. Because SPYCE has higher accuracy for coarser computational grids, it takes smaller computational time than all other electrophoresis simulators to achieve the same accuracy.

3.1 Isotachophoresis (ITP)

We begin by verifying the numerical method and its implementation in SPYCE with SPRESSO's sixth-order compact adaptive scheme, using an example of isotachophoretic preconcentration and separation of four analytes. Simulations in SPYCE and SPRESSO were performed in a 40 mm long physical domain discretized with 257 grid points. The LE ion was 100 mM chloride ion, the TE ion was 100 mM HEPES, and the background counter-ion was 150 mM TRIS. Four analytes, namely, malonic acid (A1), acetic acid (A2), lactic acid (A3), and cacodylic acid (A4) were injected between the LE and TE zones in the form of diffused plugs with a maximum concentration of 20 mM each. The electrophoretic mobilities μ and acid dissociation constants (pK_a) for various chemical species used in this simulation are tabulated in Table S1. The simulation was performed for a constant current density of 1019 A/m^2, corresponding to a current of 2 μA through a 50 μm diameter circular capillary. For this simulation, we used the moving mesh to cluster the grid points in the regions with poorly resolved numerical solution. The parameters for the moving mesh method were: $\beta = 1 - 10^{-5}$, $\delta = 10^{-3}c_{max}$, and $\tau = 5 \times 10^{-3}\tau_0$, where τ_0 is the reference time-scale defined as $\tau_0 = Lc_{max}F/|j|$. Here, c_{max} denotes the maximum species concentration at the initial state and F is the Faraday constant. The adaptive grid parameters of SPRESSO, namely the adaptive grid speed and the clustering level, were both chosen to be one to ensure a non-oscillatory solution. The computational times required by SPYCE and SPRESSO for this problem were about 15 and 30 s, respectively.

Figure 1 shows the comparison of simulation predictions using the Chebyshev pseudo-spectral method implemented in SPYCE and the sixth-order compact scheme of SPRESSO. Initially ($t = 0$ s), the four analytes with equal concentrations are injected between the LE and TE zones. Upon application of electric field, the analytes begin to separate into distinct zones. At intermediate times ($t = 150$ s), separation and preconcentration is characterized by mixed analyte zones. At later times ($t = 300$ s), the analytes separate into purified plateau-shaped zones. As shown in Figure 1, the spatio-temporal variation of the species concentrations predicted by the Chebyshev pseudo-spectral method matches with that predicted by the experimentally validated SPRESSO simulator, thereby verifying the implementation of the numerical method.

Next, we compare the performance of the grid adaptation scheme in SPYCE, which is based on clustering the grid points in the regions with poor numerical resolution with that in SPRESSO wherein grid points are clustered in the regions with large concentration gradients. In Figure 2, we plot the spatio-temporal evolution of the grid points and electrical conductivity on a t versus x diagram. The background color corresponds to the electrical conductivity, and the lines correspond to the position of grid points in the physical domain. For clarity, we have plotted every second grid point in Figure 2. The spatio-temporal evolution of conductivity predicted by SPYCE is same as that predicted by SPRESSO. Moreover,

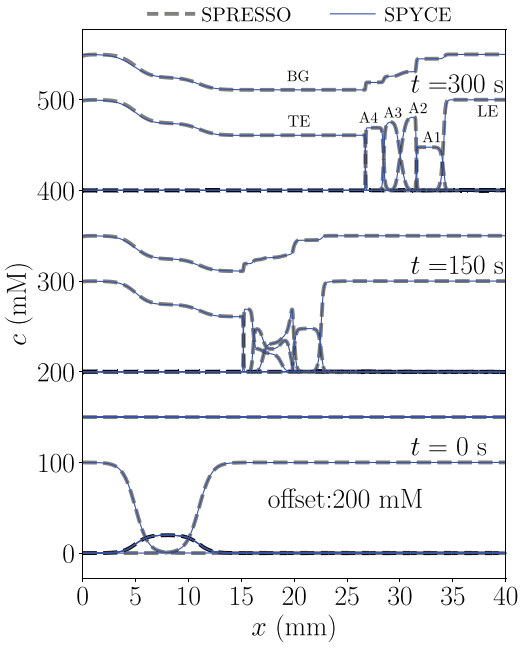

Figure 1. Simulation of ITP preconcentration and separation of four analytes using the Chebyshev pseudo-spectral method with moving mesh and its verification with the sixth-order compact adaptive scheme of SPRESSO. The concentrations predicted by the Chebyshev pseudo-spectral method agree well with those simulated by SPRESSO, verifying the implementation of the numerical scheme in SPYCE.

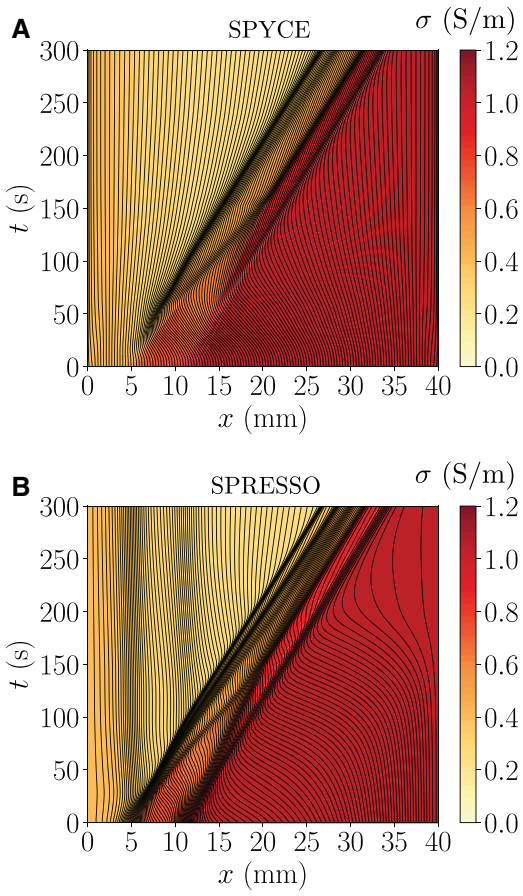

Figure 2. Comparison of conductivity field and grid adaptation in SPYCE and SPRESSO for the ITP simulation shown in Fig. 1. The conductivity field, shown in background color, predicted by SPYCE agrees with that obtained from SPRESSO. (A) The grid points in SPYCE are made to cluster in the regions with poor numerical resolution, whereas (B) in SPRESSO the grid density increases in the regions with concentration gradients. The moving mesh method of SPYCE clusters grid points only in the regions where higher grid density is required to improve the solution accuracy. On the other hand, SPRESSO's adaptive grid scheme unnecessarily clusters grid points even in the regions with gradual concentration gradients, such as at $x = 5$, 10 mm.

the grid points cluster at the locations of sharp concentration gradients separating analyte zones in both the simulations. However, there are notable differences in the grid movement in the two simulations. SPRESSO's grid adaptation scheme, based on a gradient-based monitor function, also clusters grid points at the locations with smooth concentration gradients. For example, Figure 2B shows that the gradient-based monitor function of SPRESSO leads to clustering of grid points at $x = 5, 10$ mm, where the TE concentration adapts from its initial value upon displacing the analytes. In contrast, the monitor function based on the high-pass filter in SPYCE does not cluster the grid points in such regions, as the numerical solution there is well-resolved despite low grid density. Overall, a comparison of grid movement in Figure 2A and B shows that the numerical scheme described here requires lesser grid movement compared with that required by SPRESSO to yield a non-oscillatory solution. Besides the difference in the monitor functions, lesser grid movement in the simulation using SPYCE is also because the Chebyshev pseudo-spectral method can better resolve the high-wavenumber features than the sixth-order compact scheme of SPRESSO.

3.2 Isoelectric focusing

Next, we present a simulation of IEF, which involves separation of amphoteric species based on the differences in their isoelectric points (pI). We also validate the predictions of SPYCE with those using COMSOL's electrophoretic transport interface, described in detail by Mikkonen et al. [11]. We considered 21 hypothetical carrier ampholytes with pI values ranging between 4 and 9 ($\Delta \mathrm{p}I = 0.25$) and $\Delta \mathrm{p}K_a = 2$ for each ampholyte. All the ampholytes were assumed to have the same absolute value of mobility, $\mu_{i,\pm 1} = \pm 30 \times 10^{-9}$ m^2/Vs. The simulation was performed for a 20 mm long, closed column with impermeable ends. The column was discretized with 1025 grid points in SPYCE. Because IEF involves many concentration gradients distributed throughout the column, the moving mesh does not help in improving the computational speed. Therefore, this simulation was performed on a stationary and almost uniform grid using the arcsine map given by Equation (9) with $\beta = 1 - 10^{-7}$. The same conditions were used to perform finite element method (FEM)

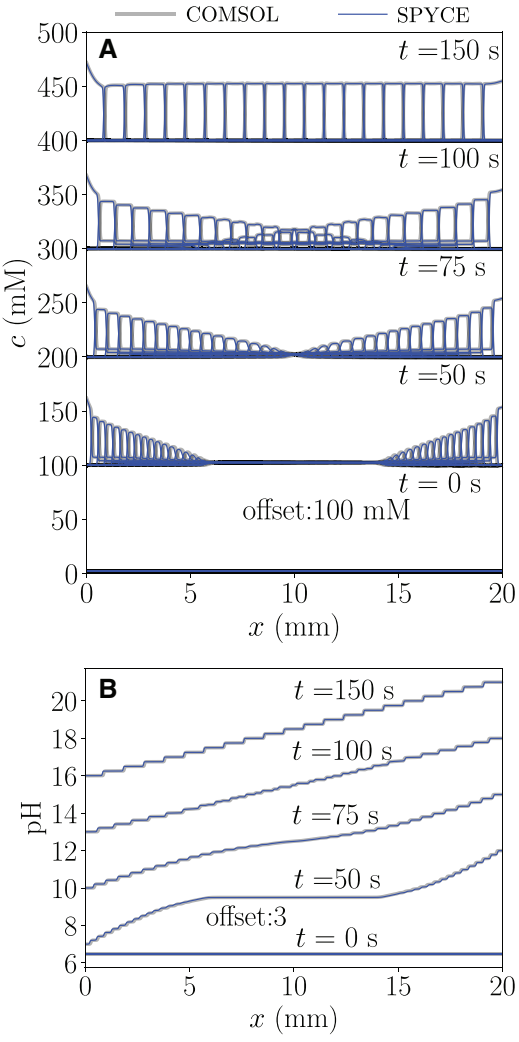

Figure 3. Time-evolution of the distribution of ampholyte concentrations and pH in IEF simulated using the Chebyshev pseudo-spectral method in SPYCE and FEM in COMSOL. The simulation was performed in a closed column to demonstrate the compatibility of the numerical method for impenetrable boundaries. (A) Initially, the 21 model ampholytes are distributed uniformly in the column. The application of electric field causes the analytes to separate into distinct zones ordered by their pI. (B) Initially, uniform pH of 6.5 gives way to a steady, step variation of pH upon application of the electric field. The predictions of SPYCE agree well with those of COMSOL.

based simulations in COMSOL, except that that column was discretized into 3075 grid points in COMSOL. These FEM simulations used linear and quadratic shape functions for concentrations and electric potential, respectively, and backward difference formula (BDF) based time integration.

Initially ($t = 0$), all the ampholytes were mixed uniformly in the column, each having an initial concentration of 2.5 mM as shown in Figure 3A. This initial condition corresponds to a uniform pH of 6.5, as shown in Fig. 3B. For $t > 0$, the current density was ramped up over 0 s to 12 s to a maximum value of 509 A/m^2 and thereafter held constant till $t = 150$ s. Figure 3A and B shows the spatio-temporal evolution of the ampholyte concentrations and the pH, respectively. At the initial pH of 6.5, ampholytes having pI between 4 and 6.25 are positively charged, the ampholyte with p$I = 6.5$ is electrically neutral, while those with pI between 6.75 and 9 are negatively charged. Therefore, the ampholytes with pI between 4 and 6.25 migrate toward the anode, while those with pI between 6.75 and 9 migrate toward the cathode. Simultaneously, the local pH adapts to balance the charge due to the movement of ampholytes. Over time, these ampholytes accumulate at the respective ends in the form of separate zones ordered by their pI, as shown in Figure 3A. At the steady-state, the pH in the individual zones is equal to the pI of the respective ampholyte (Fig. 3B), and consequently the ampholytes are neutrally charged in their respective zones away from the zone boundaries [28]. Figure 3 shows that the spatio-temporal evolution of species concentrations and the pH predicted by SPYCE agree with the predictions of COMSOL. Because of the large number of grid points and species in this IEF simulation, SPYCE took 16 min to complete the simulation.

The results of ITP and IEF simulations in Figures 1 and 3, and CZE simulations in the Supporting Information demonstrate the ability of the adaptive Chebyshev pseudo-spectral method to accurately simulate electrophoretic phenomena in nonperiodic domains with open and closed boundaries. We note that the Chebyshev pseudo-spectral method is also applicable for simulating other electrophoretic processes such as FASS, t-ITP, and oscillating electrolytes whose simulations we presented earlier on a periodic domain using the Fourier pseudo-spectral method [10]. The input files for performing ITP, IEF, and CZE simulations presented here, and those for performing simulations of FASS, t-ITP, and oscillating electrolytes are available along with the SPYCE package.

4 Concluding remarks

We have demonstrated the ability of Chebyshev pseudo-spectral method coupled with a moving mesh scheme to perform high-resolution numerical simulations of nonlinear electrophoretic processes on a nonperiodic domain. Unlike the Fourier pseudo-spectral method, implemented earlier in the SPYCE simulator, this numerical method is not restricted to a periodic domain. Consequently, the adaptive Chebyshev pseudo-spectral method is applicable for simulating a wider variety of electrophoresis techniques in channels with open and closed boundaries. Moreover, this method retains the advantages of the Fourier pseudo-spectral method, including high accuracy and computationally efficient implementation based on FFT. Further improvement in computational efficiency is achieved using a novel moving mesh scheme, which clusters the grid points in the regions with poor numerical resolution. This grid-adaptation approach allows simulations of electrophoretic processes in long domains with relatively fewer grid points. Moreover, this grid-adaptation approach avoids unnecessary clustering of grid points in

regions with well-resolved concentration gradients, unlike the schemes based on clustering the grid points in regions with concentration gradients.

Based on the examples of ITP, IEF, and CZE, we have demonstrated the applicability of the adaptive Chebyshev pseudo-spectral method for simulating electrophoresis techniques at current densities as high as 1000 A/m^2. We have implemented this scheme in the SPYCE simulator and verified it with the existing electrophoresis simulators, including SPRESSO, SIMUL, and COMSOL's electrophoretic transport interface. The updated SPYCE simulator can now simulate all 1D electrophoresis processes, including ITP, t-ITP, IEF, CZE, FASS, and oscillating electrolytes with high accuracy and low computational time. The Chebyshev pseudo-spectral method has the highest accuracy compared with the other finite-difference schemes, such as the second-order central differencing scheme used in SIMUL and GENTRANS, sixth-order compact scheme used in SPRESSO, and finite element method used in COMSOL. Therefore, the SPYCE simulator based on the Chebyshev pseudo-spectral method on adaptive grid offers the highest numerical accuracy among all the electrophoresis simulators.

S.S.B. gratefully acknowledges the financial support received from the Science and Engineering Research Board (SERB), Government of India, under Impacting Research Innovation and Technology (IMPRINT-2) Scheme (Grant No. IMP/2018/000422).

The authors have declared no conflict of interest.

Data availability statement

Data available on request from the authors.

5 References

[1] Thormann, W., Caslavska, J., Breadmore, M. C., Mosher, R. A., *Electrophoresis* 2009, *30*, S16–S26.

[2] Thormann, W., Mosher, R. A., *Electrophoresis* 2022, *43*, 10–36.

[3] Jorgenson, J. W., Lukacs, K. D., *Science* 1983, *222*, 266–274.

[4] Everaerts, F. M., Beckers, J. L., Verheggen, T. P., *Isotachophoresis: Theory, Instrumentation and Applications*, Elsevier, Amsterdam 2011.

[5] Bahga, S. S., Santiago, J. G., *Analyst* 2013, *138*, 735–754.

[6] Righetti, P. G., *Isoelectric focusing: theory, methodology and application*, Elsevier, Amsterdam 2000.

[7] Bharadwaj, R., Santiago, J. G., *J. Fluid Mech.* 2005, *543*, 57–92.

[8] Gaš, B., Bravenec, P., *Electrophoresis* 2021, *42*, 1291–1299.

[9] Bercovici, M., Lele, S. K., Santiago, J. G., *J. Chromatogr. A* 2009, *1216*, 1008–1018.

[10] Gupta, P., Bahga, S. S., *Electrophoresis* 2021, *42*, 890–898.

[11] Mikkonen, S., Ekström, H., Thormann, W., *J. Chromatogr. A* 2018, *1532*, 216–222.

[12] Bier, M., Palusinski, O., Mosher, R., Saville, D., *Science* 1983, *219*, 1281–1287.

[13] Saville, D., Palusinski, O., *AIChE Journal* 1986, *32*, 207–214.

[14] Bahga, S. S., Bercovici, M., Santiago, J. G., *Electrophoresis* 2010, *31*, 910–919.

[15] Mosher, R. A., Dewey, D., Thormann, W., Saville, D. A., Bier, M., *Anal. Chem.* 1989, *61*, 362–366.

[16] Bahga, S. S., Bercovici, M., Santiago, J. G., *Electrophoresis* 2012, *33*, 3036–3051.

[17] Thormann, W., Zhang, C.-X., Caslavska, J., Gebauer, P., Mosher, R. A., *Anal. Chem.* 1998, *70*, 549–562.

[18] Trefethen, L. N., *Spectral methods in MATLAB*, Society for Industrial and Applied Mathematics, Philadelphia 2000.

[19] Boyd, J. P., *Chebyshev and Fourier spectral methods*, Dover Publications, Mineola, NY 2001.

[20] Fornberg, B., *SIAM J Numer. Anal.* 1990, *27*, 904–918.

[21] Hruška, V., Jaroš, M., Gaš, B., *Electrophoresis* 2006, *27*, 513–518.

[22] Gupta, P., Bahga, S. S., *Phys. Rev. E: Stat. Nonlinear Soft Matter Phys.* 2015, *92*, 022301.

[23] Kosloff, D., Tal-Ezer, H., *J. Comput. Phys.* 1993, *104*, 457–469.

[24] Subich, C. J., *J. Comput. Phys.* 2015, *294*, 297–311.

[25] Beckett, G., Mackenzie, J., Ramage, A., Sloan, D., *J. Comput. Phys.* 2001, *167*, 372–392.

[26] Mulholland, L., Qiu, Y., Sloan, D., *J. Comput. Phys.* 1997, *131*, 280–298.

[27] Hou, T. Y., Li, R., *J. Comput. Phys.* 2007, *226*, 379–397.

[28] Thormann, W., Mosher, R. A., *Electrophoresis* 2021, *42*, 814–833.

